Improvements of Satellite-Derived Cyclonic Rainfall over the North Atlantic

CHRISTIAN-PHILIPP KLEPP

Max-Planck-Institut für Meteorologie, and Meteorologisches Institut, Universität Hamburg, Hamburg, Germany

STEPHAN BAKAN

Max-Planck-Institut für Meteorologie, Hamburg, Germany

HARTMUT GRAßL

Max-Planck-Institut für Meteorologie, and Meteorologisches Institut, Universität Hamburg, Hamburg, Germany

(Manuscript received 8 November 2001, in final form 3 July 2002)

ABSTRACT

Case studies of rainfall, derived from Special Sensor Microwave Imager (SSM/I) satellite data during the passage of individual cyclones over the North Atlantic, are presented to enhance the knowledge of rainfall processes associated with frontal systems. A multisatellite method is applied for complete coverage of the North Atlantic twice a day. Different SSM/I precipitation algorithms have been tested for individual cyclones and compared to the Global Precipitation Climatology Project (GPCP) datasets. An independent rainfall pattern and intensity validation method is presented using voluntary observing ship (VOS) datasets and Advanced Very High Resolution Radiometer (AVHRR) images.

Intense cyclones occur frequently in the wintertime period, with cold fronts propagating far south over the North Atlantic. Following upstream, large cloud clusters are frequently embedded in the cellular structured cold air of the backside regions, which produce heavy convective rainfall events, especially in the region off Newfoundland around 50°N. These storms can be easily identified on AVHRR images. It transpired that only the SSM/I rainfall algorithm of Bauer and Schlüssel is sensitive enough to detect the rainfall patterns and intensities observed by VOS for those cyclone types over the North Atlantic. In contrast, the GPCP products do not recognize this backside rainfall, whereas the frontal rainfall conditions are well represented in all tested datasets. This is suggested from the results of an intensive intercomparison study with ship reports from the time period of the Fronts and Atlantic Storm Track Experiment (FASTEX) field campaign. For this purpose, a new technique has been developed to transfer ship report codes into rain-rate estimates. From the analysis of a complete life cycle of a cyclone, it follows that these mesoscale backside rainfall events contribute up to 25% to the total amount of rainfall in North Atlantic cyclones.

1. Introduction

The water and energy cycle plays an important role in the climate system, as shown by the World Climate Research Program's (WCRP's) Global Energy and Water Cycle Experiment (GEWEX). However, several components of the water and energy cycle are not yet sufficiently understood. In particular, the insufficient description of rainfall processes is one of the key problems in existing deficiencies of climate simulation (Houghton et al. 1995). The extremely localized and intermittent nature of rain processes poses considerable problems for the derivation of reliable climatological fields. To obtain these together with other climatically relevant parameters on a global scale, satellite data have become one major source of information. However, remote sensing data only provide an indirect measure of the required quantity—in our case the rain rate at the earth's surface—through the application of appropriate algorithms. Although these are usually derived from basic physical principles, they require independent in situ surface observations for validation. These are especially difficult to collect over the world's oceans due to the usually sparse observation density. In the framework of concerted studies on the climate-related causes and consequences of the North Atlantic Oscillation, the present paper focuses on the quality of rainfall estimated from satellite data for midlatitude cyclones. The atmospheric part of the water cycle over the midlatitude oceans is primarily driven by water exchange in cyclones. The North Atlantic is a key region in global climate coupling, as the global conveyor belt system is triggered

Corresponding author address: Dr. Christian-Philipp Klepp, Max-Planck-Institut für Meteorologie, Bundesstr. 55, 20146 Hamburg, Germany.
E-mail: klepp@dkrz.de

within this region. This system is sensitive to the amount of freshwater on the ocean surface produced by precipitation. In addition, large horizontal SST gradients exist in this region and result in large air–sea temperature gradients causing intense convection and rainfall.

To study individual North Atlantic cyclones using satellites, good spatial and temporal resolution with high-quality data over the entire region is needed. However, existing analyses of individual cyclones are mostly based on field experiments like the Fronts and Atlantic Storm Track Experiment (FASTEX; Joly et al. 1997). Data from such experiments are valuable for validation, but do not allow the sampling of entire cyclones and their life cycles. Therefore, satellite-derived investigations of water cycle parameters, especially the precipitation rate, of individual cyclones over the North Atlantic are presented on a case study basis. Here, the rainfall rate during individual overpasses of the satellites is validated with in situ data from voluntary observing ships (VOS) including high-quality observations from FASTEX in January and February 1997 (Klepp and Bakan 2000).

Microwave satellite data from the Special Sensor Microwave Imager (SSM/I) on board the Defense Meteorological Satellite Program (DMSP) platforms are essential to derive precipitation fields over the global oceans (Wentz 1991). This is due to the fairly homogeneous emissivity of the ocean surface and the ability of microwave radiation to penetrate through even raining and iced clouds. Related remote sensing datasets like the Hamburg Ocean–Atmosphere Parameters and Fluxes from Satellite Data (HOAPS; Graßl et al. 2000; Jost et al. 2002) or the Global Precipitation Climatology Project (GPCP; Huffman et al. 1997) supply essential contributions to this topic. Both climatologies primarily provide monthly mean data and climatological mean values. Additional individual orbit datasets are limited to single satellite data products that cannot be used for the investigation of individual cyclones and their life cycle. This is due to the fact that single-satellite swaths cover the earth's surface only partly, leaving large data gaps especially near the equator. In this paper a method is used to combine precipitation estimates from three SSM/I platforms for complete data coverage of the North Atlantic twice a day.

The major goal of this investigation is to evaluate the applicability of available precipitation algorithms to individual satellite scenes, with useful accuracy to document the spatial distribution and temporal development of precipitation fields in North Atlantic cyclones. Many of the considered algorithms have been intercompared and validated in the algorithm and precipitation intercomparison projects (AIP and PIP; Ebert 1996; Smith et al. 1998). A significant number of these algorithms were developed and validated mostly for tropical conditions on an instantaneous and monthly mean basis (Ebert and Manton 1998) and then applied globally. In the present paper the performance of the four well-known algorithms from Bauer and Schlüssel (1993, hereafter called SBSA for SSM/I Bauer and Schlüssel algorithm), Ferraro and Marks (1995), Wentz (1991), and the Goddard Profiling Algorithm (GPROF; Kummerow et al. 2001) is investigated for the derivation of North Atlantic precipitation fields. These are applied to the stratiform and convective cyclone rainfall types: warm fronts, cyclogenesis, cold fronts, and cold convective backside rainfall, which occurs frequently behind cold fronts following the post frontal subsidence. In addition, the rainfall representation in the combined satellite data sets of GPCP (Huffman et al. 1997) is evaluated. Differences between the various derived precipitation fields of North Atlantic cyclones are assessed using VOS benchmark data. As these in situ data do not include a direct observation of rain rates, a rainfall allocation is developed between the VOS rainfall type and the corresponding rainfall rate. The results of 10 typical winter cyclone case studies in January and February 1997 are presented in this paper. The precipitation fields and analysis for the above-mentioned algorithm results are presented for the cyclone on 17 February 1997, which is not even the strongest of the 10 events studied.

The derivation of the total amount of rainfall in typical North Atlantic cyclones focuses on the error impact in the freshwater flux resulting from the systematic absence of the backside rainfall. A solution to this problem is described in order to obtain more realistic rainfall results (Klepp 2001).

2. Data sources

The major data source used in the present study for remote sensing of precipitation in North Atlantic cyclones is the SSM/I data from three different platforms, namely, *F10*, *F11*, and *F13*, obtained from the National Oceanic and Atmospheric Administration (NOAA) National Environmental Satellite, Data, and Information Service (NESDIS). The investigated time interval corresponds to the FASTEX field experiment in January and February 1997 because of the increased number of observation ships for the North Atlantic that produced many additional high-quality observations. The aim of the field experiment FASTEX was to investigate individual cyclones, their life cycle, and the impact on the European coasts (Joly et al. 1997). Furthermore, cyclones from November 1992 and March 1993 contributing to the database were also investigated. The rain-rate algorithms of Bauer and Schlüssel (1993), Ferraro and Marks (1995), Wentz (1991), and GPCP GPROF (Kummerow et al. 2001) are applied to these datasets.

Externally processed data sources came from the GPCP (Huffman et al. 1997) and the remote sensing database of Wentz (see online at http://www.ssmi.com). The GPCP individual orbit and combined daily merged data products are provided online at http://rsd.gsfc.nasa.gov/912/gpcp/. The latter dataset is a companion to the GPCP version 2, called the global One-Degree

Daily (1DD) product and consists of merged global, 3-hourly, infrared, brightness temperature histograms on a $1° \times 1°$ grid in the band 40°N–40°S. The dataset uses SSM/I data, GPCP version 2 satellite–gauge combination, geosynchronous-orbit infrared data, low-orbit infrared Geostationary Operational Environmental Satellite (GOES) Precipitation Index (GPI), and the Television Infrared Observational Satellite (TIROS) Operational Vertical Sounder (TOVS) data (Susskind et al. 1997). GPCP states that there is good continuity across the 40°N, S data boundary (Huffman et al. 1997).

Additionally, the GPROF algorithm in the version 4.0 and 6.0 was tested against the SSM/I Bauer algorithm. GPROF is a physically based retrieval of hydrometeor (vertical) profiles that best fit the available channels of passive radiometer data (Kummerow et al. 1996). Rainfall algorithms are usually based mainly on either an emission or scattering technique. The emission-based technique uses the low frequencies of the radiometer at 19 GHz for low-level rainfall detection. The estimation of rainfall comes directly from the emission of raindrops in the lower atmosphere that dominate the signal.

When the clouds become more convective and ice particles dominate the upper layers of the clouds, such as cirrus fields over convective clusters, the estimation of rainfall becomes more indirect using the scattering technique with frequencies of 85 GHz (Bauer and Schlüssel 1993). The SBSA technique uses a channel combination of both the emission and scattering frequencies that might be sensitive to all rainfall types within the life cycle of North Atlantic cyclones. Therefore the brightness temperatures of all channels are used to derive a set of parameters dependent on the atmospheric situation by using an adopted scheme of individual regressions for cloud-free, cloudy, and raining atmospheres over the ocean. At first, the total water path is calculated. Values smaller than 0.005 g cm^{-2} are treated as cloud free and the integrated water vapor is calculated. If the total water path exceeds the threshold of 0.005 g cm^{-2} but the rain rate remains below a threshold of 0.3 mm h^{-1} the atmosphere is considered cloudy but nonraining. In this case the integrated water vapor, liquid, and ice water content are calculated with a second set of algorithms. Above the rain-rate threshold of 0.3 mm h^{-1}, a third set of regression algorithms is used to calculate all parameter values. It is important to mention that the SBSA algorithm was developed and calibrated with a set of radiosonde profiles that cover all latitudes from polar regions to the Tropics in order to be representative for global conditions.

Advanced Very High Resolution Radiometer (AVHRR) infrared data is used for identifying cloud clusters on satellite images and the SST data is processed from the NOAA Pathfinder dataset. The VOS data is provided by the European Centre for Medium-Range Weather Forecasts (ECMWF), stored in the original raw data format that is independent of any calculated model output.

3. Multisatellite method

Individual extratropical cyclones over the global ocean have so far only been investigated on a single-satellite basis. The use of single-satellite orbits for individual cyclones anywhere over the midlatitude oceans results in large spatial and temporal data gaps. Therefore, the investigation of individual cyclones and their life cycle is considerably hampered (Fig. 1a). During the investigation period in winter 1997, data of three suitable passive microwave polar-orbiting satellite radiometers (*F10, F11,* and *F13*) were available for combination into complete aerial coverage. Merging these data into a combined product yields complete data coverage of the North Atlantic twice a day. The satellite *F13* was selected as the reference because its equator crossing time between 0600 and 1200 UTC fits best to the in situ VOS data. Remaining data gaps are filled with data of the *F11* satellite, which passes the North Atlantic 2 h and 21 min later than *F13.* The remaining small data gaps are filled by *F10* another 72 min later. The resulting structure of the highly variable parameter precipitation shows the successful use of the multisatellite method over the North Atlantic (Fig. 1b).

4. Results

a. Rainfall algorithm intercomparison study

Especially in the winter, the North Atlantic is a key region in the earth's climate system. The dominating Gulf Stream advects warm water up to 20°C to the northeast where it comes into contact with the polar water mass of the Labrador Sea off the coast of Newfoundland. Horizontal differences in sea surface temperature (SST) up to 15°C across a 200-km horizontal scale result in very large SST gradients (Fig. 2). This region exhibits a maximum in precipitation and evaporation that is related to the area of frequent intensive cyclogenesis.

Figure 3a shows the rainfall rate as calculated from SSM/I data using the SBSA. A mature cyclone was located over the North Atlantic on 17 February 1997 with a warm front propagating over the United Kingdom and a cold front off the coast of Ireland. Intense midlevel convection occurs behind the well-developed postfrontal subsidence west of the cold front causing heavy precipitation in a large cluster and two additional rain bands to the southeast of Greenland. These intense rainfall patterns to the west of mature cold fronts occur nearly every three days in wintertime, whenever a mature cyclone system leads to a cold air outflow west of the cold front. This feature will be called ''backside rainfall'' in the following. Infrared and visible AVHRR scenes always indicate large convective clusters in this specific region off the coast of Newfoundland that are embedded in the cellular convection (Fig. 4). Additionally, a typical cyclogenesis is visible off the east coast of the United States as well as a subtropical shower system at 20°N.

These results using SBSA were compared to the well-

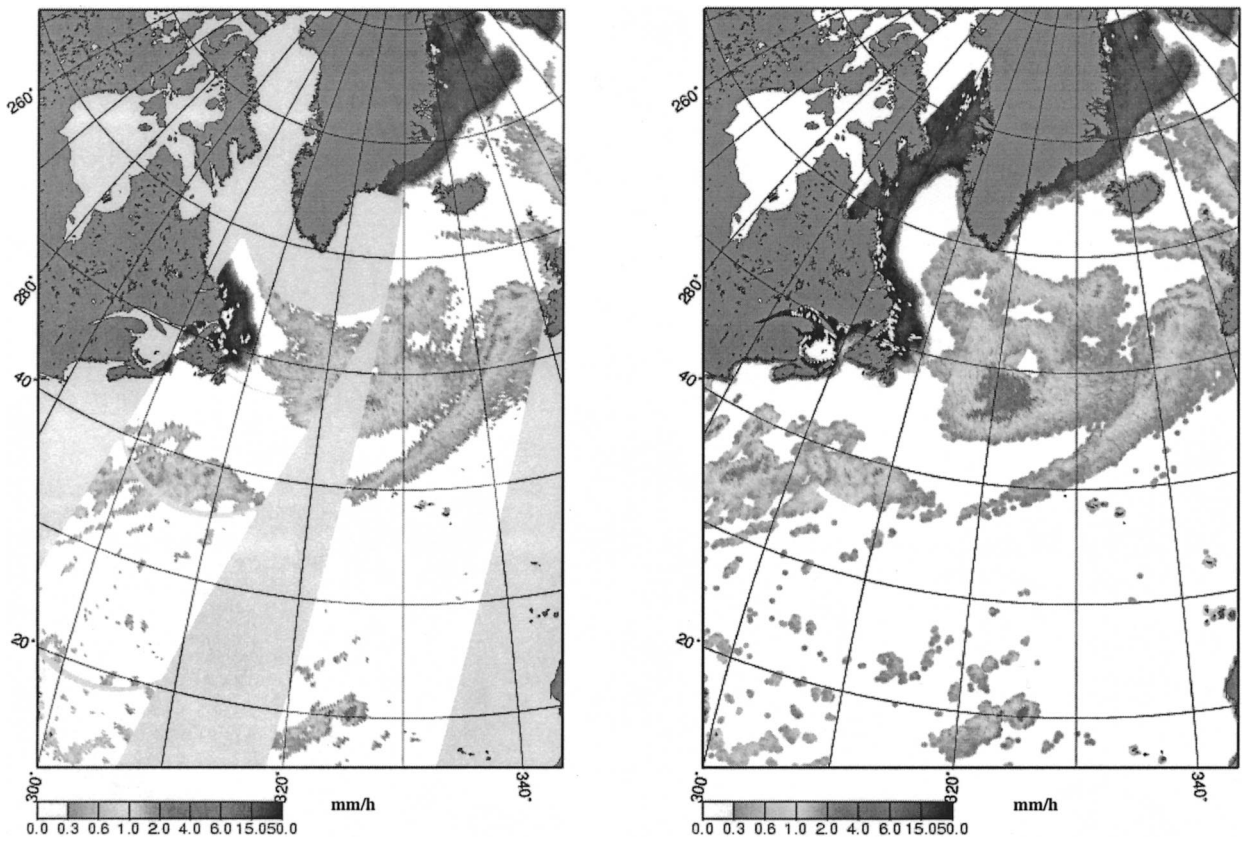

FIG. 1. The SBSA precipitation rate for 17 Feb 1997 in mm h^{-1} using (a) a single-satellite (*F11*) and (b) using the multisatellite method. The ice margin is visible along the coastal lines in the north.

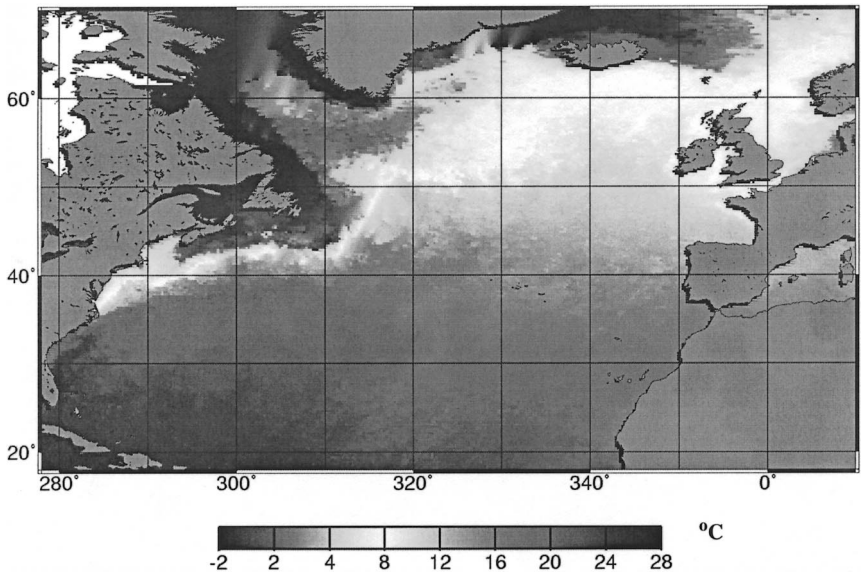

FIG. 2. NOAA Pathfinder SST in °C for the fourth pentad in Feb 1997. Note the back-tilted SST structure heading toward the Davis Strait, indicating the area with strongest SST gradients.

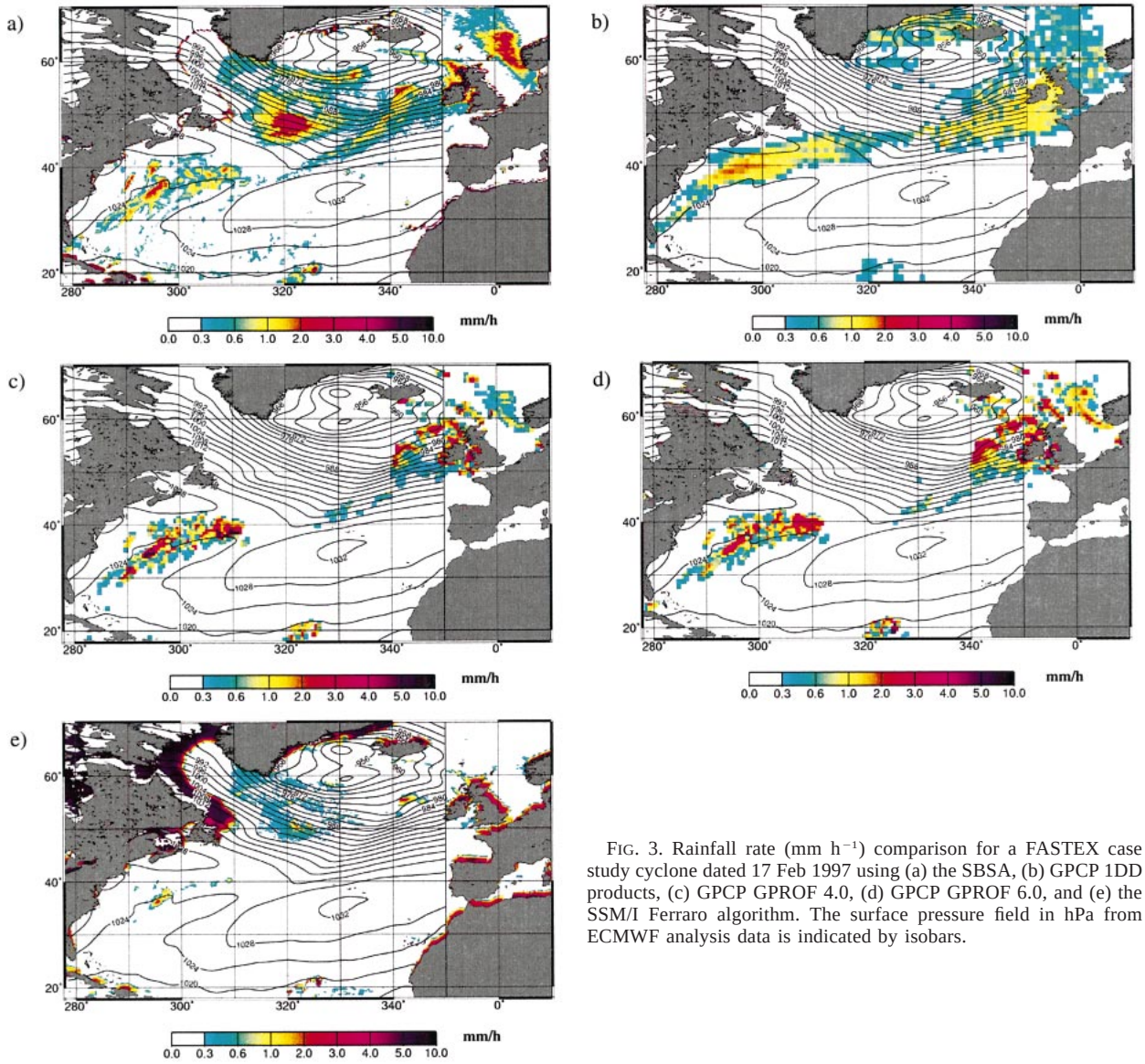

FIG. 3. Rainfall rate (mm h^{-1}) comparison for a FASTEX case study cyclone dated 17 Feb 1997 using (a) the SBSA, (b) GPCP 1DD products, (c) GPCP GPROF 4.0, (d) GPCP GPROF 6.0, and (e) the SSM/I Ferraro algorithm. The surface pressure field in hPa from ECMWF analysis data is indicated by isobars.

established rainfall climatology GPCP, for which the rain rates of all three available data products (1DD, GPROF 4.0, and GPROF 6.0) are displayed in Figs. 3b–d. Although GPCP uses a merged satellite dataset, the data sources poleward of 40°N and 40°S are limited to SSM/I data only. Comparing the frontal rainfall structures leads to the conclusion that the GPCP products generally coincide well with the SBSA rainfall pattern, whereas the rainfall intensity even exceeds the values derived by the SBSA. The GPROF 6.0 algorithm provides even higher values than GPROF 4.0, while the 1DD product gives lower values due to its daily averaged basis. However, the situation is different with the backside rainfall, which is not notably picked up by the various versions of the GPCP products. This major difference was also found in many other cyclone cases in this area of the North Atlantic.

To assess this difference between the GPCP products and those of the SBSA, two additional SSM/I rainfall algorithms were tested, the scattering index method of Ferraro and Marks (1995; Fig. 3e) and the unified all-weather algorithm of Wentz (1997). While the Wentz algorithm behaves similar to the GPCP products in neglecting the backside rainfall completely, the Ferraro algorithm turns out to neglect the frontal structures except for the most intense rainfall centers. The backside rainfall pattern is found to be quite similar to the SBSA pattern, but the rainfall intensity in this area is vastly underestimated.

The precipitation climatology HOAPS (Jost et al.

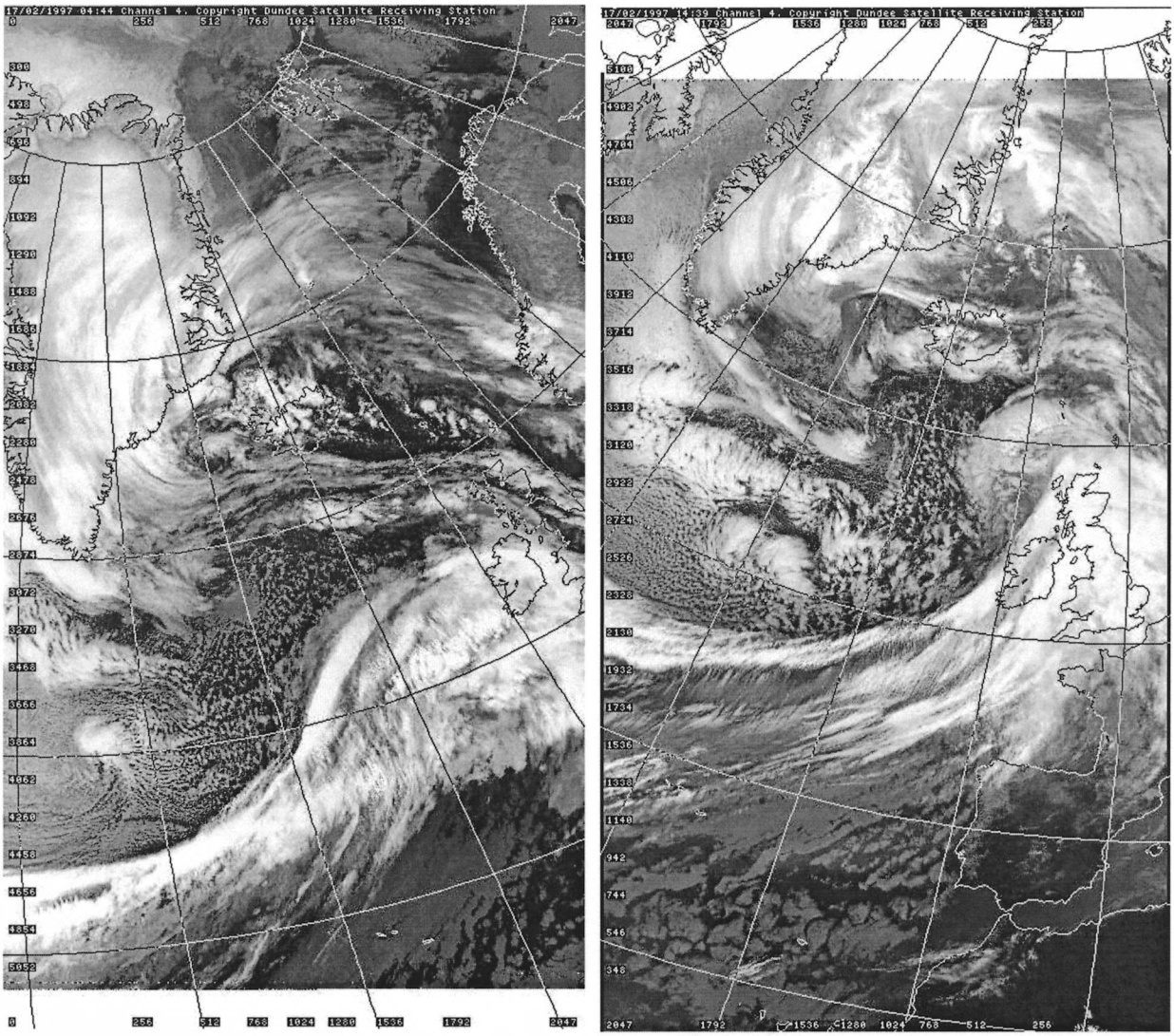

FIG. 4. Infrared AVHRR channel 4 satellite image dated 17 Feb 1997, (a) 0444 UTC and (b) 1439 UTC. Highly convective cloud bands are embedded in the cellular cloud structure west of the cold front (source: http://www.sat.dundee.ac.uk/).

2002), which is also based on SBSA, shows an intense rain band off the east coast of the United States over the Gulf Stream. Off the coast of Newfoundland the rainband structure is tilted backward toward the Davis Strait (Fig. 5). This area, which marks the preferred position of the heavy convective backside rainfall that occurs over the region with the largest SST gradients (Fig. 3a), was identified in all case studies investigated for November 1992, March 1993, and January–February 1997. These rain clusters are always embedded into the cellular cloud structure observed in the airflow of the cold air outbreaks through the Davis Strait. It is remarkable that the rainfall intensity reduces considerably as soon as the cyclones are advected over regions with lower SST gradients in the eastern Atlantic.

b. VOS precipitation validation

In view of the extremely different results for the backside rain events off the coast of Newfoundland produced by different rain algorithms, a validation study has been carried out with in situ data from VOSs. Ten typical case studies have been selected that all exhibit typical backside rainfall patterns over the North Atlantic, as shown by the SBSA results. For this purpose, a total of 101 VOS rainfall observations are available. The dataset was subdivided into the major areas of cyclonic rainfall resulting in 37 VOS observations in cold fronts, 40 in the backside rainfall region, 9 in the region of permanent cyclogenesis off the east coast of the United States, 11 in warm fronts, and 4 in subtropical shower systems.

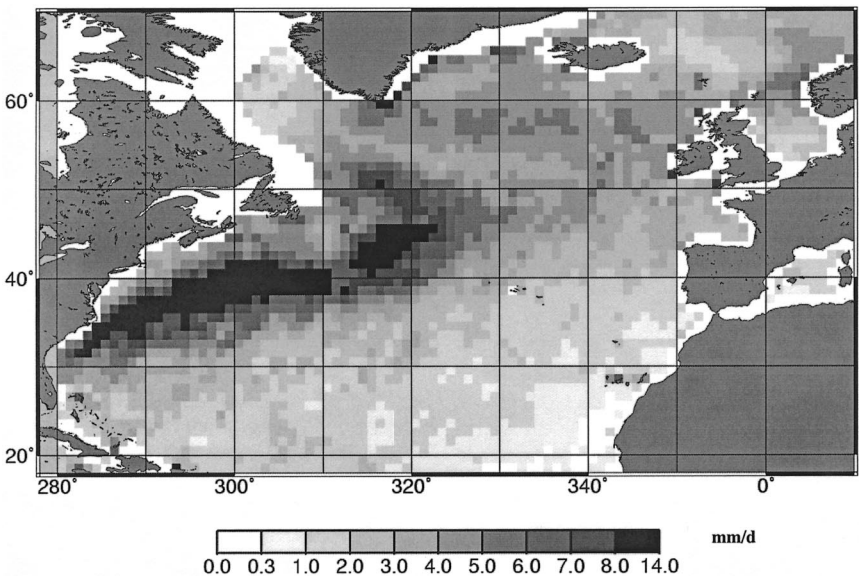

FIG. 5. The climatological Feb precipitation mean in mm day^{-1} between 1988 and 1999, derived from HOAPS data.

Figure 6 displays the SSM/I Bauer rainfall rate versus all other tested datasets for every grid point where a VOS rainfall code exists for all 10 case studies separately for the different cyclonic areas. Although a large data scatter is visible, the expected correlation between the results of the different algorithms exists for cold fronts, cyclogenesis, and warm fronts. However, significant differences occur for the case of cold backsides, where the SBSA gives fairly high rainfall rates in comparison with all other datasets (Fig. 6c).

In order to determine the circumstances of this disagreement between different satellite algorithms, the VOS data are further exploited. The present weather-code table described in the ECMWF binary universal form for the representation of meteorological data (BUFR) tables provides detailed information about the observed rainfall situation. Therefore, the available VOS rainfall observations have been analyzed by splitting them into rainfall types for each cyclone region. Table 1 shows that cold fronts are characterized by observations of various shower and rain types, while reports of drizzle and light rain prevail in warm front cases. In comparison to this it is remarkable that on the cold convective backsides of mature cyclones, 17 of 40 VOS rainfall observations are labeled as heavy convective precipitation by the local observer, often including VOS codes like ''violent rain showers.'' This result gives independent indication that these backside rainfall patterns really exist, as suggested by the SBSA results.

Figure 7 presents the SBSA rain rates and related VOS codes for a typical backside rainfall case study from 9 February 1997. The time shift between the *F13* pass and the VOS codes is less than 1 h in this case. None of the GPCP products indicates rain in the whole area shown in Fig. 7, whereas the SBSA results indicate large areas of rainfall including patches of intense rainfall. This rain distribution compares well with the overlaid VOS rainfall codes. All VOS no-rain observations match the SBSA remote sensing data and each VOS rainfall observation has an appropriate remote sensing rainfall value similar to the SBSA. High rainfall values correspond well with VOS codes representing heavy convective showers including thunderstorms, if the shift of rain areas between satellite overpass and VOS observation time is accounted for.

The next validation step tests the plausibility of the SBSA rainfall intensity estimates in the convective cold air clusters. As the VOS observations do not provide rainfall rate data, the observed VOS present weather codes have to be converted into calibrated rainfall classes. The Tucker algorithm (Tucker 1961), which is used in the Comprehensive Ocean–Atmosphere Data Set (COADS) to convert VOS codes to rainfall rates, restricts higher rainfall rates to an upper limit of 2.7 mm h^{-1} in the midlatitudes (Jost 2000). Comparison of this limit with rain rate values of all remote sensing rainfall products of the present study (cf. Fig. 6) indicates that the Tucker algorithm tends to underestimate the rainfall over the North Atlantic in all regions of the cyclones. Therefore, a similar scheme is developed for the present study that uses the whole range of rainfall intensity from all analyzed products (GPCP, 1DD, GPROF 4.0, as well as Ferraro and Wentz) and cyclone areas for every VOS data point. But to be sure of an independent procedure, the SBSA results are not used, nor are any results from the backside rainfall areas included. Seven rainfall classes are defined from light drizzle (0.3 mm h^{-1}) to violent rain showers (exceeding 5 mm h^{-1}) covering the range of observed VOS codes and derived rainfall rates. A

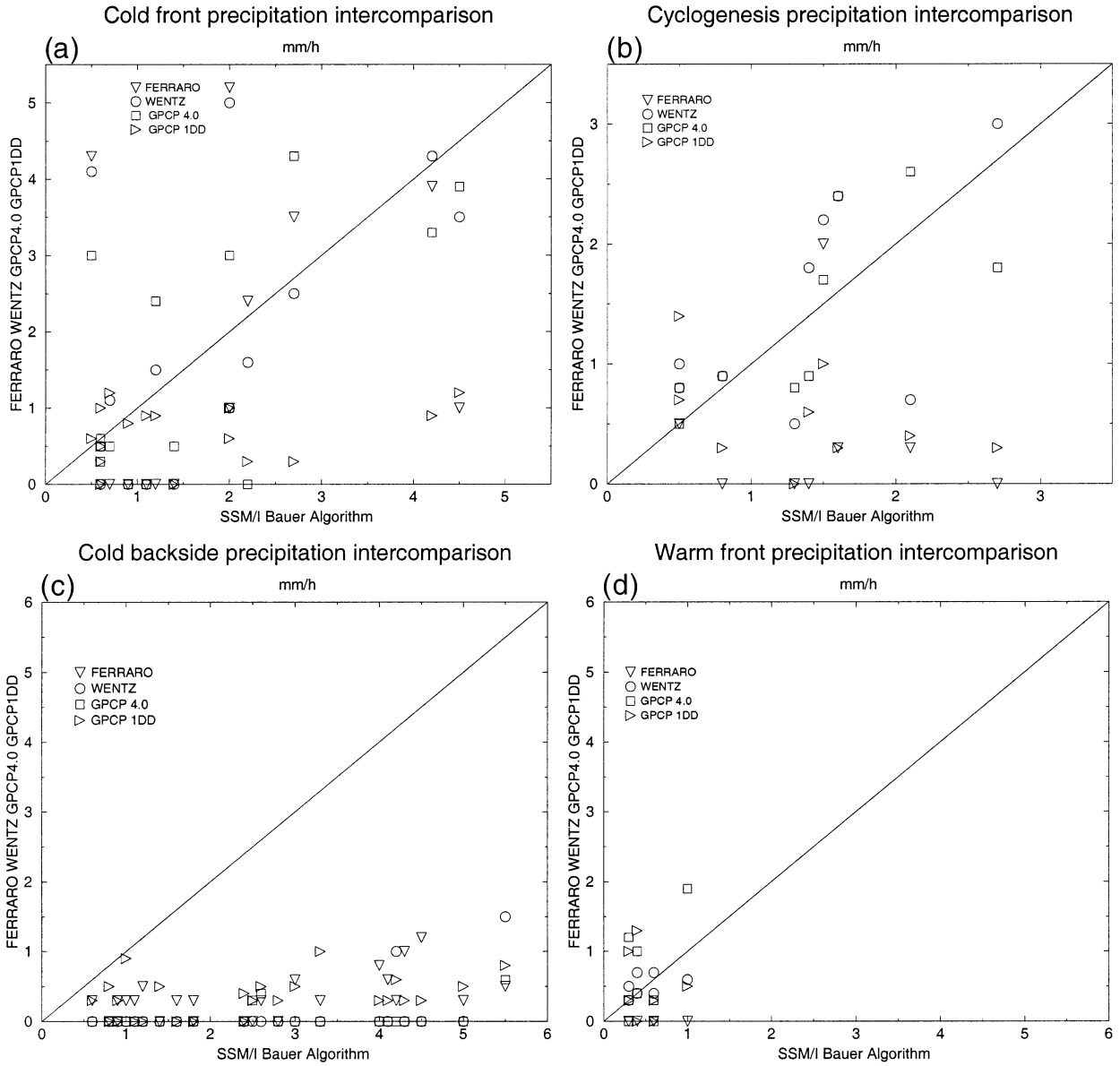

FIG. 6. Precipitation comparison for 10 typical case studies in mm h^{-1} between the SBSA and all other tested datasets, separated into the cyclone regions (a) cold fronts, (b) cyclogenesis, (c) cold backsides, and (d) warm fronts.

TABLE 1. Observed VOS rainfall types for 10 case studies separated into cyclone regions.

Category	Cold fronts	Backsides	Cyclogenesis	Warm fronts
Thunderstorm			1	
Heavy showers	6	17	1	
Heavy rain	2			
Moderate showers		3		
Moderate rain	6	6	1	
Light showers	12	6	1	1
Light rain	5	3	2	3
Drizzle (all types)	6	5	3	7
Total observations	37	40	9	11

mean remote sensing rain-rate value is calculated for each VOS rainfall grid point from the available satellite rainfall rates (without SBSA results) and the corresponding VOS codes are associated with one of the seven basic categories (Table 2).

Figure 8 displays the satellite versus the newly constructed VOS rainfall rate. Despite the remaining scatter, fairly good agreement between VOS and remote sensing rainfall rates is displayed in cold fronts, warm fronts, and cyclogenesis areas. This is not too surprising for all the considered algorithms except for the SBSA, as they have been used to derive the relationship. It is, however, reassuring that the SBSA results also correspond similarly well to the VOS rain rates. In the case of the cold

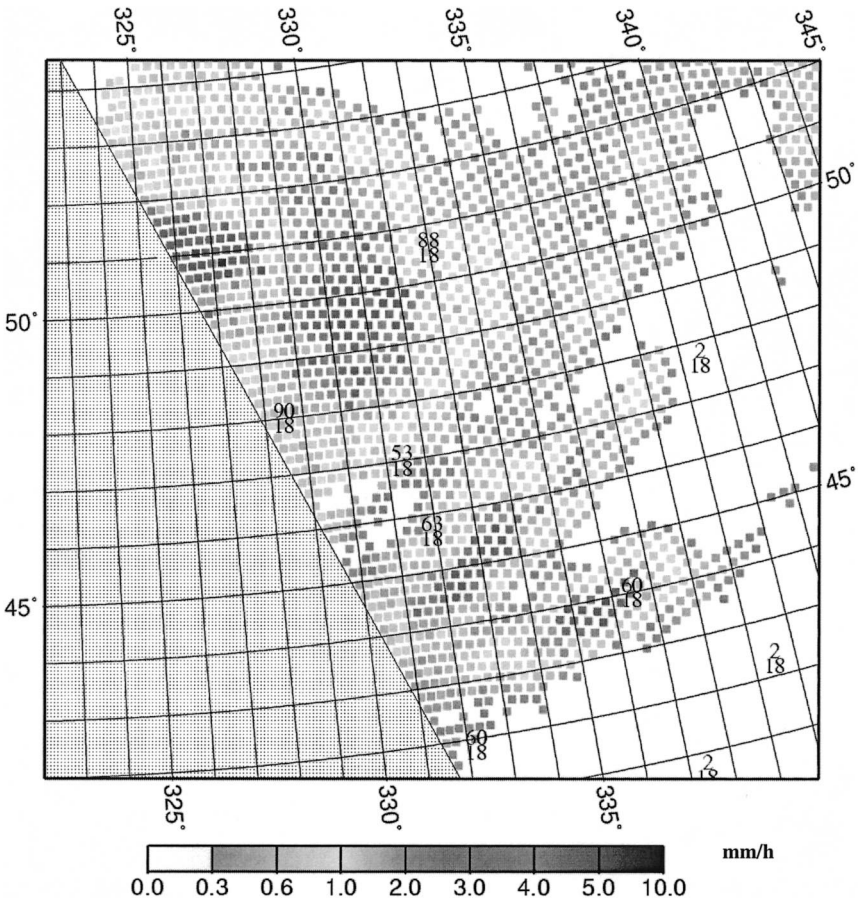

FIG. 7. The SBSA precipitation rate for 9 Feb 1997 1858 UTC (mm h^{-1}) overlaid by the VOS codes from 1800 UTC (digits). The gray shaded area indicates missing satellite data coverage. VOS code 2 indicates no rain, 53 = drizzle, 60 = light rain, 63 = moderate rain, 88 = heavy shower, and 90 = thunderstorm with heavy shower.

backside, however, (Fig. 8c) it is clearly visible that only the SBSA rainfall rates, indicated by stars, scatter around the VOS-observed values. The other datasets mostly underestimate the rainfall rates or do not recognize rain at all. This underestimation gets even more pronounced when rainfall rates are averaged within each of the seven defined rainfall classes as shown in Fig. 9.

TABLE 2. Conversion of VOS rainfall reports into seven rainfall classes.

Rainfall class	Rain rate (mm h^{-1})	VOS codes
Light drizzle	0.3	50, 51, 78
Moderate drizzle	0.4–0.6	20, 52, 53
Heavy drizzle	0.7–1.0	55, 56, 57, 153
Light rain (showers)	1.1–2.0	16, 26, 60, 61, 71, 72, 80, 83, 87, 98, 180, 185, 186
Moderate rain (showers)	2.1–3.0	15, 21, 25, 62, 63, 84, 86, 88, 162, 173
Heavy rain (showers)	3.1–4.9	81, 89, 163
Violent rain showers	>5.0	82, 90

From these results we conclude that only the SBSA is able to produce reasonable rainfall patterns and intensities on the cold backsides of mature cyclones and all other cyclone regions. For a short discussion of possible reasons see section 5.

c. Total amount of rainfall

The SBSA together with the multisatellite method described in section 3 allows an estimation of the total amount of rainfall during a complete life cycle of North Atlantic cyclones. This knowledge is essential for estimations of the water balance and freshwater input into the ocean. It also provides an indication of the importance of the mentioned backside rainfall for the water balance of a cyclone. Figure 10 presents the total amount of rainfall as well as the precipitation area, mean, and maximum precipitation for the case study cyclone between 13 and 21 February 1997. The data from 17 February 1997, used as a typical example in this study, represent the mature stage of the cyclone as it passed the central North Atlantic on its way toward Europe. However, it did not cross the

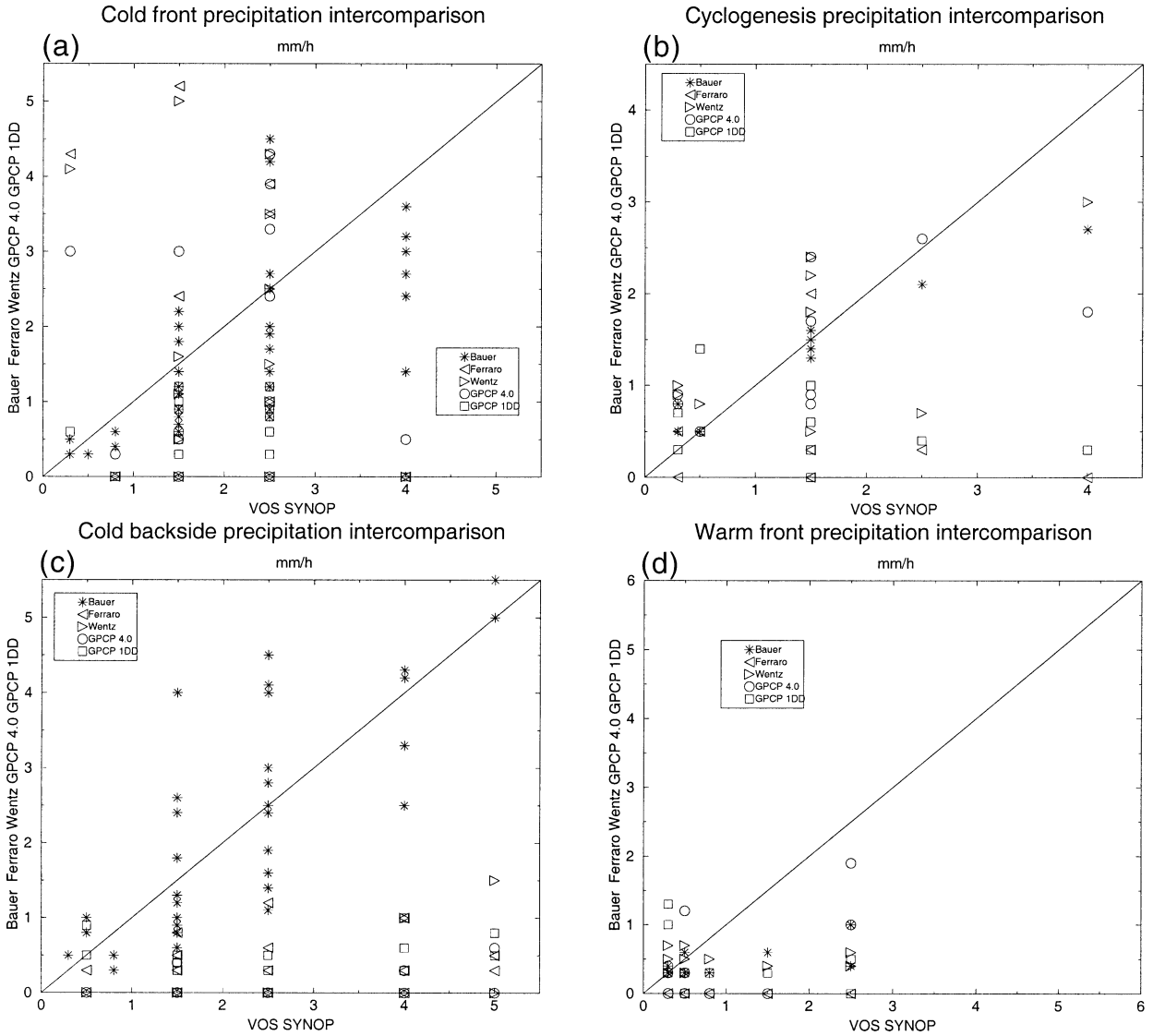

FIG. 8. Precipitation comparison for 10 typical case studies in mm h^{-1} between the independent VOS data and all other tested datasets separated into the cyclone region (a) cold fronts, (b) cyclogenesis, (c) cold backsides, and (d) warm fronts.

European continent but was advected on a retrograde track toward southeast Greenland where the cyclone dissolved. This special cyclone track made it possible to calculate the total amount of rainfall throughout the complete life cycle. This is usually impossible because cyclones tend to cross the European continent and the estimation of rainfall over land is of doubtful accuracy using microwave satellite data.

The total amount of rainfall increases rapidly as the cyclone develops off the coast of the United States over the Gulf Stream. On 17 February 1997, the cyclone was advected over the central North Atlantic, deepening strongly (cf. Fig. 3a). The above-discussed backside rainfall event develops within 12 h and contributes up to 60% of the instantaneous rainfall amount of the entire cyclone (black part of the column in Fig. 10a). The cold front contributes up to 25%, the warm front up to 15% of the total amount of rainfall. Over the full life cycle of the cyclone the backside rainfall contributes up to 25% of the total rainfall. It is however a fairly short-lived phenomena that becomes unimportant after 24 h, when the entire cyclone degenerates rapidly to small rainfall rates and amounts. This points out clearly the importance and potential impact of these backside rainfall events for the entire cyclone. There is good correlation between the rainfall area (Fig. 10b) and the total amount of rainfall, which is not the case for the mean and maximum precipitation (Figs. 10c,d). The mean and the maximum instantaneous precipitation are highest as long as the cyclogenesis state is limited to the strong

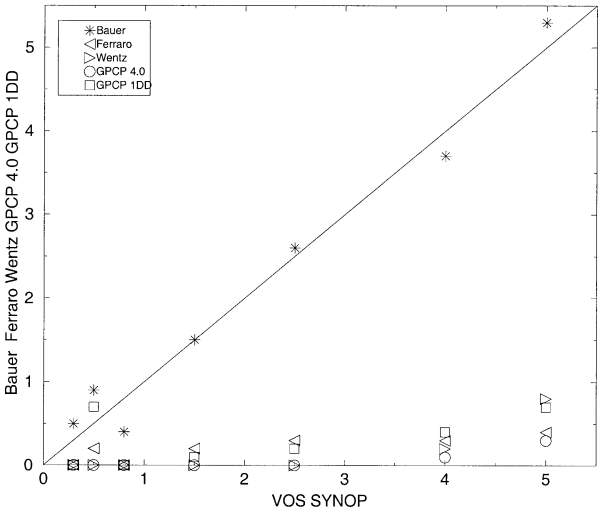

FIG. 9. Cold backside precipitation comparison averaged over the rainfall classes for each dataset in mm h^{-1}.

SST gradient region over the Gulf Stream off the northeast coast of the United States. The maximum precipitation rate exceeds 14 mm h^{-1} two days before the mature state of the entire cyclone. Even the backside rainfall rates never reach these high rainfall values and are mostly limited to a maximum of 6 mm h^{-1}.

The total amount of rainfall during the complete life cycle of this cyclone produced about 3.9×10^{11} m^3 of freshwater input into the ocean within 8 days. The backside contributes about 1 Sv [1 Sverdrup (Sv) $\equiv 10^6$ m^3 s^{-1}] of freshwater instantaneously into a region where up to now it was not believed to rain at all. As mentioned earlier, this phenomenon occurs on the backside of virtually every cyclone in this region during the winter. This additional input of 1 Sv of freshwater nearly every three days must have an impact on salinity balance of the North Atlantic Ocean in this region.

5. Discussion and conclusions

Precipitation fields were derived for individual cyclones over the North Atlantic using SSM/I data. A multisatellite method has been applied that allows data from three satellites to merge for a complete coverage over the North Atlantic twice a day.

Intense rainfall occurs approximately every three days on the backside of mature cyclones within the cold airflow over the North Atlantic off the coast of Newfoundland. Only the SSM/I Bauer and Schlüssel algorithm proved to be sensitive enough to detect these rainfall events. Visible and infrared AVHRR images show large convective cloud clusters in these regions. The area of intense convective rainfall is highly correlated with the region of strongest gradients in sea surface temperature between the Gulf Stream and the polar water mass of the Labrador Sea. The remotely sensed rainfall was successfully validated with in situ VOS data, establishing a relation between the present weather code and the rainfall rate. GPCP products proved to represent frontal rainfall patterns without any problems, but the convective backside rainfall remains unrecognized.

The reason for these strong differences between the algorithms is difficult to assess. For one, the brightness temperature images of all SSM/I channels reveal the backside rainfall area clearly in contrast to the surrounding sea surface. But the various rain-rate algorithms generally use brightness temperature differences between various channels, which complicates the problem assessment further. The SBSA rain-rate formula, for example, contains five terms, of which three are of similar size and tend to compensate each other such that the two remaining smaller terms provide an important contribution to the result. One of these contains the 85-GHz channel that is crucially determined by scattering processes.

On the other hand, the maximum brightness temperature in the backside cloud area are in all channels considerably smaller than most values in the frontal and cyclogenetic regions. This fact might lead to the exclusion of these apparently too cold backside regions from the rain-rate analysis in algorithms that use a brightness temperature threshold technique. This might be the case in algorithms being originally developed for the analysis of tropical precipitation. It is, however, difficult to find out to what extent such thresholds are used in the various codes. The SBSA method, in contrast, uses a cloud screening of the scene with a threshold of the estimated total water column followed by another threshold of the derived rain rate itself. To what extent this may be the reason for the experienced differences in derived rain rates could only be decided in a larger algorithm intercomparison effort that was beyond the scope of the present study.

The total amount of rainfall during the life cycle of typical cyclones over the North Atlantic may reach and even exceed 4×10^{11} m^3. The backside rainfall contributes instantaneously up to 60% and up to 25% in total to the amount of rainfall of a typical cyclone. By following a cyclone through the complete life cycle it transpired that the total amount of rainfall is mostly determined by the precipitation area and not so much by the mean or maximum precipitation in any stage.

When looking for the possible reasons for the occurrence of such intense backside rainfall events, significant sea level pressure reductions up to 16 hPa were found in the local VOS reports of the backside rainfall areas compared to the surrounding pressure field. This indicates strong local cyclogenesis that often remains unrecognized in the ECMWF analysis (Klepp 2001; C. Klepp et al. 2002, unpublished manuscript).

These results encourage further analysis of the water balance components of cyclones through their life cycle. This should help to quantify the contribution of cyclones to the global atmospheric energy and water balance.

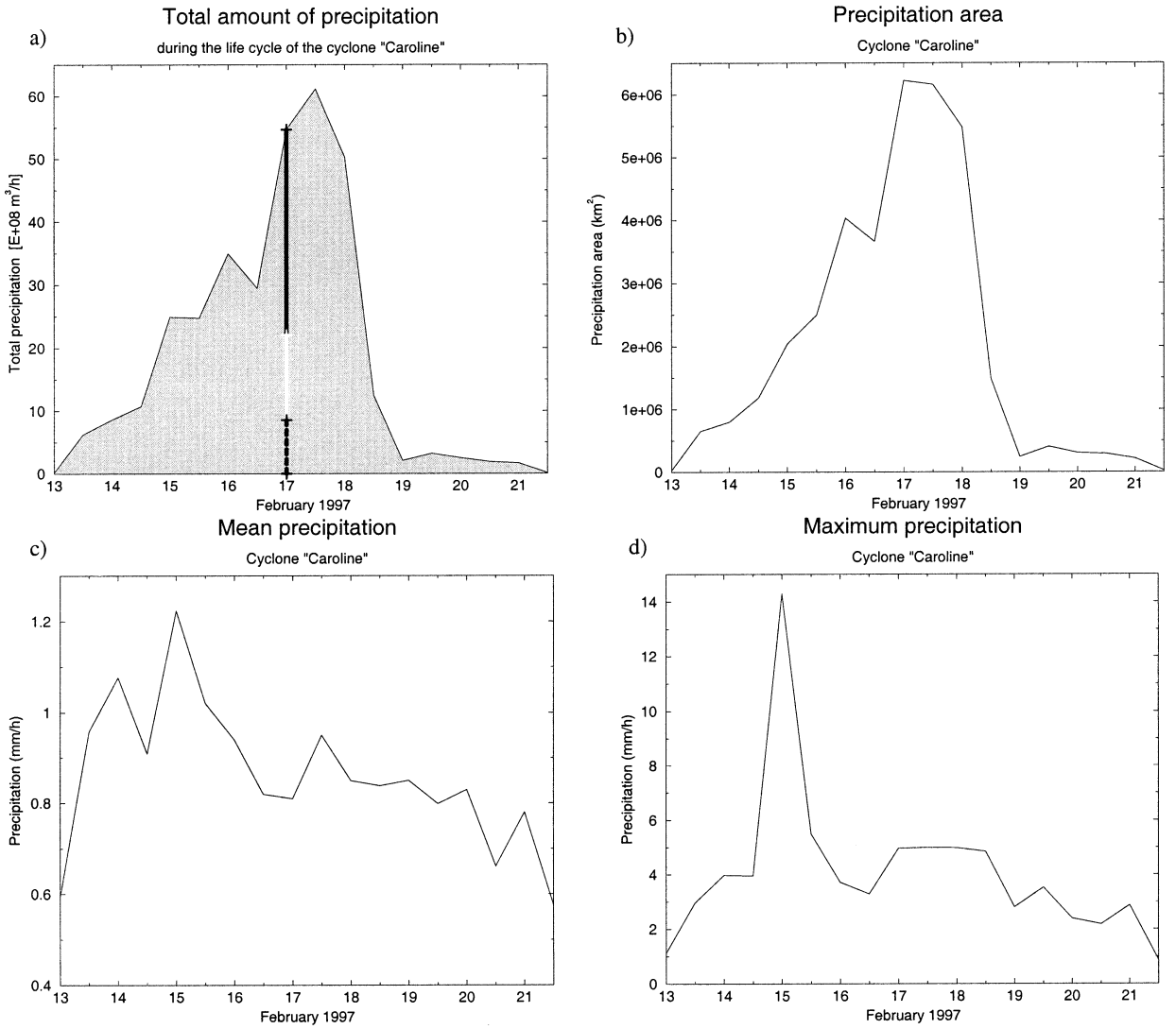

FIG. 10. Total amount of (a) rainfall, (b) precipitation area, (c) mean precipitation, and (d) maximum precipitation for the complete life cycle of the case study cyclone between 13 and 21 Feb 1997. The vertical column in (a) indicates the precipitation contribution by the cold backside (black), the cold front (white), and the warm front (dashed) in the mature state of the cyclone at 17 Feb 1997.

Acknowledgments. This study was funded by the Sonderforschungsbereich 512 (granted by the Deutsche Forschungsgemeinschaft to the Universität Hamburg) and the Max-Planck Institute für Meteorologie, Hamburg, Germany. We thank Peter Bauer for valuable comments.

REFERENCES

Bauer, P., and P. Schlüssel, 1993: Rainfall, total water, ice water and water vapor over sea from polarized microwave simulations and Special Sensor Microwave/Imager data. *J. Geophys. Res.,* **98** (D11), 20 737–20 759.

Ebert, E., 1996: Results of the 3rd Algorithm Intercomparison Project (AIP-3) of the Global Precipitation Climatology Project (GPCP). Revision 1. BMRC Research Rep. 55, 299 pp.

——, and A. Manton, 1998: Performance of satellite rainfall estimations algorithms during TOGA/COARE. *J. Atmos. Sci.,* **55,** 1537–1557.

Ferraro, R., and G. Marks, 1995: The development of SSM/I rain rate retrieval algorithms using ground-based radar measurements. *J. Atmos. Oceanic Technol.,* **12,** 755–770.

Graßl, H., V. Jost, J. Schulz, R. Kumar, P. Bauer, and P. Schlüssel, 2000: A climatological atlas of satellite-derived air–sea interaction parameters over the worlds ocean. Max-Planck Rep. 312, Max-Planck Institute for Meteorology, Hamburg, Germany, 120 pp.

Houghton, J. T., L. G. Meira Filho, J. P. Bruce, H. Lee, B. A. Callander, and E. F. Haites, Eds.,1995: *Climate Change 1994: Radiative Forcing of Climate Change and an Evaluation of the IPCC IS92 Emission Scenarios.* Cambridge University Press, 347 pp.

Huffman, G., and Coauthors, 1997: The Global Precipitation Climatology Project (GPCP) combined precipitation dataset. *Bull. Amer. Meteor. Soc.,* **78,** 5–20.

Joly, A., D. Jorgensen, M. Shapiro, A. Thorpe, P. Bessemoulin, and K. Browning, 1997: The Fronts and Atlantic Storm-Track Experiment (FASTEX): Scientific objectives and experimental design. *Bull. Amer. Meteor. Soc.,* **78,** 1917–1940.

Jost, V., 2000: HOAPS: Eine neue Klimatologie des Süßwasserflusses

an der Meeresoberfläche abgeleitet aus Satellitendaten. Ph.D. dissertation, Universität Hamburg, 133 pp.
——, S. Bakan, and K. Fennig, 2002: HOAPS—A new satellite-derived freshwater flux climatology. *Meteor. Z.,* **11,** 61–70.
Klepp, C., 2001: Komponenten des Wasserkreislaufs in Zyklonen aus Satellitendaten Niederschlagsfallstudien. Ph.D. dissertation, Max-Planck Institut for Meteorology, Hamburg, Germany, 161 pp.
——, and S. Bakan, 2000: Satellite derived energy and water cycle components in North Atlantic cyclones. *Phys. Chem. Earth,* **25B,** 65–68.
Kummerow, C., W. S. Olson, and L. Giglio, 1996: A simplified scheme for obtaining precipitation and vertical hydrometeor profiles from passive microwave sensors. *IEEE Trans. Geosci. Remote Sens.,* **34,** 1213–1232.
——, and Coauthors, 2001: The evolution of the Goddard Profiling Algorithm (GPROF) for rainfall estimation from passive microwave sensors. *J. Appl. Meteor.,* **40,** 1801–1820.
Smith, E., and Coauthors, 1998: Results of the WetNet PIP-2 project. *J. Atmos. Sci.,* **55,** 1483–1536.
Susskind, J., P. Piraino, L. Rokke, L. Iredell, and A. Mehta, 1997: Characteristics of the TOVS Pathfinder Path A Dataset. *Bull. Amer. Meteor. Soc.,* **78,** 1449–1472.
Tucker, G. B., 1961: Precipitation over the North Atlantic Ocean. *Quart. J. Roy. Meteor. Soc.,* **87,** 147–158.
Wentz, F., 1991: User's manual SSM/I antenna temperature geophysical tapes. Tech. Rep. 120191, Remote Sensing Systems, Santa Rosa, CA, 70 pp.
——, 1997: A well-calibrated ocean algorithm for special sensor microwave/imager. *J. Geophys. Res.,* **102** (C4), 8703–8718.